ACS OMEGA

Article

http://pubs.acs.org/journal/acsodf

Immobilization of Neurotrophin Peptides on Gold Nanoparticles by Direct and Lipid-Mediated Interaction: A New Multipotential Therapeutic Nanoplatform for CNS Disorders

Patrizia Di Pietro,[†] Nunzia Caporarello,[‡] Carmelina D. Anfuso,[‡] Gabriella Lupo,[‡] Antonio Magrì,[§] Diego La Mendola,*[,∥] and Cristina Satriano*[,†]

[†]Department of Chemical Sciences, University of Catania, Viale Andrea Doria, 6, 95125 Catania, Italy

[‡]Department of Biomedical and Biotechnological Sciences, University of Catania, Biological Tower, Via Santa Sofia 97, 95123 Catania, Italy

[§]Institute of Biostructures and Bioimages − Catania, National Council of Research (IBB-CNR), Via Paolo Gaifami, 16, I-95125 Catania, Italy

[∥]Department of Pharmacy, University of Pisa, via Bonanno Pisano, 6, I-56100 Pisa, Italy

Supporting Information

ABSTRACT: Neurotrophins are essential proteins for the development and maintenance of neural functions as well as promising drugs in neurodegenerative disorders. Current limits in their effective clinical applications can be overwhelmed by the combined use of peptidomimetic and nanomedicine approaches. Indeed, neurotrophin-mimicking peptides may allow minimizing the adverse side effects of the whole protein drug. Moreover, the immobilization of such peptides on nanomaterials may offer additional advantages, including protection against degradation, enhanced permeability of barrier membranes, and intrinsic therapeutic properties of the nanoparticles (e.g., antiangiogenic and plasmonic features of gold nanoparticles (AuNPs)). In the present article, we scrutinize the functionalization of spherical AuNPs of diameter 12 nm by peptides because of the N-terminal domains of the nerve growth factor (NGF) and the brain-derived neurotrophic factor (BDNF), NGF1-14 and BDNF1-12, respectively. The hybrid gold−peptide nanobiointerface was investigated, both in the direct physisorption and in the lipid-bilayer-mediated adsorption processes, by a multitechnique study that included UV−vis and X-ray photoelectron spectroscopies, dynamic light scattering, zeta-potential analyses, and atomic force microscopy. Both peptide- and lipid-dependent features were identified, to have a modulation in the peptide coverage of nanoparticles as well as in the cellular uptake of NGF and BDNF peptides, as investigated by confocal microscopy. The promising potentials of the neurotrophins to cross the blood−brain barrier were demonstrated.

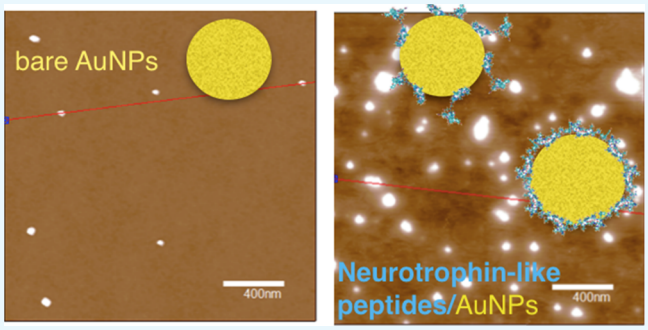

1. INTRODUCTION

Nanoparticle-based platforms have recently attracted much attention for the delivery of drugs and molecules with neuroprotective and regenerative activities that, under normal conditions, cannot pass through the blood−brain barrier (BBB), the vital interface between the neural tissue and circulating blood.[1,2]

Neurotrophin proteins, produced by the cells of the central nervous system (CNS), are growth factors regulating the neuron division, survival, and neurite outgrowth.[3,4] A forefront medicine research area deals with making neurotrophins a clinical reality for people suffering from disorders, involving neuronal degeneration (such as Alzheimer's, Huntington's, and Parkinson's disease)[5−7] and physical trauma resulting in the severing of nerve connections (i.e., accidents and sports-related injuries).[8]

Despite the great potential of neurotrophic factors in the therapeutic action, their clinical application has been so far limited because of their poor plasma stability, low penetration of the BBB, and serious side effects, such as pain.[9,10] So far, only few cases of neurotrophin-based drugs have been approved for use in humans, that is, for administering opioids in chronic pain management and as antisplasticity drugs for spinal cord injury.[8]

The potential of neurotrophin-based drugs can be enhanced by new hybrid systems comprising (1) peptides capable of mimicking the whole proteins by retaining their functionality of neurotrophic action[11] and (2) nanoparticles capable of binding the neurotrophin-like drug by either physical or chemical

Received: April 14, 2017
Accepted: May 26, 2017
Published: August 1, 2017

DOI: 10.1021/acsomega.7b00458
ACS Omega 2017, 2, 4071−4079

immobilization,[12,13] where the drug-delivery capability and the ability to cross the BBB could be finely controlled over their size, surface charge, hydrophobicity, shape, coating, and chemistry.[1,14−17]

We have recently demonstrated that peptide sequences NGF1-14 and BDNF1-12, which encompass the N-terminal domain of nerve growth factor (NGF) and brain-derived neurotrophic factor (BDNF), respectively, exhibit neurotrophin-mimicking capabilities also upon immobilization on the solid gold surface.[18,19] In the present study, we move a step forward on the fabrication and biological validation of the hybrid nanobiointerface established between neurotrophin peptides and gold nanoparticles (AuNPs) that represents an attractive scaffold to construct a multifaceted theranostic platform (Scheme 1).

Scheme 1. Representative Picture of the Hybrid AuNP−Peptide Interface for a Submonolayer or Monolayer Coverage by NGF_pF (a) and $BDNF_pF$ (b) Peptides

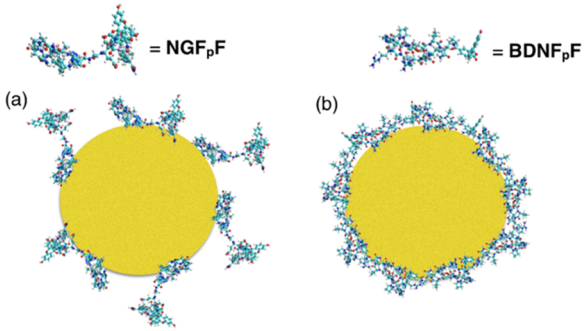

Indeed, AuNPs provide an excellent nanocarrier for the modulation of interfacial processes in biological and material applications.[20] For example, AuNPs possess intrinsic antiangiogenic[21] and anti-inflammatory activities;[22] also, because of their plasmonic properties, they are suitable for light-triggered response (e.g., hyperthermia in tumor treatment[23]) and optical imaging (biosensing[24,25]). Furthermore, drug-functionalized AuNPs might be able to cross the BBB and allow for a target-specific delivery of the active molecules to the neurons of the CNS.[15]

In general, AuNPs can open highly structured tight junctions that connect endothelial cells, which are the main components of the brain microvascular anatomy, together with the basement membrane and neighboring cells,[26] including pericytes, astrocytes, neurons, and microglia (neurovascular unit).[27] Overall, they contribute to create selective permeability for the entry of molecules between the systemic circulation and nervous tissue, maintaining the CNS homeostasis.

To enhance the image-contrast capability of the newly assembled platform,[28] the NGF- and BDNF-like peptides were dye-labeled with carboxyfluorescein (Fam) through an additional lysine (K) residue at the C-terminus, to obtain SSSHPIFHRGEFSV-K-Fam (NGF_pF) and HSDPARRGELSV-K-Fam ($BDNF_pF$), respectively.

2. RESULTS AND DISCUSSION

To modulate the peptide−metal surface interaction, a dual approach, involving direct adsorption and a lipid-mediated interaction between the peptide and the gold surfaces, was used.

In the latter case, either NGF_pP or $BDNF_pF$ was loaded in small unilamellar vesicles (SUVs) of zwitterionic 1-palmitoyl-2-oleoyl-*sn*-glycero-3-phosphorylcholine (POPC), to obtain NGF_pF-PC or $BDNF_pF$-PC, respectively.

The UV−vis titration spectra in Figure 1 show that a redshift of the plasmonic band associated with a small but significant (about 10% absorbance shift) hyperchromic effect is achieved by adding peptides at increasing concentrations. It must be noted that at higher peptide concentrations ($\geq 10^{-6}$ M), as shown in Figure 1, the apparent downshift of λ is instead due to the absorption of the Fam moiety (λ_{max} ∼490 nm) from NGF_pF and $BDNF_pF$ peptides.

The saturation in the shifts of wavelength ($\Delta\lambda$) and absorbance (ΔA) is reached at the added peptide concentrations of 0.5 μM for NGF_pF and 1 μM for $BDNF_pF$, NGF_pF-PC, and $BDNF_pF$-PC. This finding suggest that at these concentrations the maximum size of the hybrid assembly comprising a metal core (AuNP) surrounded by a soft shell (peptide molecules) is obtained, as monitored in terms of the optical sensing of the hybrid interface by the plasmonic nanoparticle.

Indeed, the intensity of maximum absorbance increases and the wavelength of the localized surface plasmon resonance band peak shifts to longer wavelengths with increasing number of molecules adsorbed on the AuNP, due to the corresponding increase in the dielectric constant of the local regions near the interfaces of gold.[29,30] The parallel occurrence of these two spectral features, as shown in Figure 1, indicates that the size increase of the colloidal metal is mostly due to the "decoration" of the nanoparticle surface by the adsorbed peptide molecules rather than a partial aggregation phenomenon.[31]

Specifically, as to the direct peptide−AuNP interaction (Figure 1a,b), the plots of ΔA versus $\Delta\lambda$ exhibit a direct one-step change for NGF_pF but a two-step change for $BDNF_pF$ (see insets). Therefore, for NGF_pF−AuNP and $BDNF_pF$−AuNP interactions, the measured curve shifts likely depend on the different stages of the peptide adsorption process, which is in turn related to the possible diverse orientation/conformation of the molecules at the interface with the AuNP surface. Such a finding is in agreement with the dissimilar affinities of the two peptides toward the Au surface, as demonstrated for NGF and BDNF peptides at the interface with flat gold, resulting in viscoelastic and rigid adlayers, respectively.[18,19]

As to the lipid-mediated peptide−AuNP interaction (Figure 1c,d), a significant synergic effect from each component, that is, peptide, lipid, and AuNP, is monitored at the hybrid nanobiointerface. First, for NGF_pF-PC, the peptide concentration at equilibrium, that is, the value corresponding to the saturation in the plasmonic peak shifts, increases up to 1 μM, comparable to that of $BDNF_pF$-PC, with a corresponding calculated coverage of about 2.4×10^7 for both NGF_pF-PC−AuNP and $BDNF_pF$-PC−AuNP interfaces. This fact suggests an active role of the fluid lipid membrane in the confinement of NGF peptide at the interface with the gold surface.[32] Such an effect would prompt a more "ordered" interaction with AuNPs and therefore a higher number of molecules detected by the plasmonic sensing.

Second, the insets in Figure 1c,d show also a peptide-driven effect, as both $\Delta\lambda$ and ΔA are narrower for NGF_pF-PC than for $BDNF_pF$-PC, consistent with that observed for NGF_pF and $BDNF_pF$, respectively.

Third, the UV−vis spectra of pellets and supernatants recovered after the centrifugation step used to remove unbound

DOI: 10.1021/acsomega.7b00458
ACS Omega 2017, 2, 4071−4079

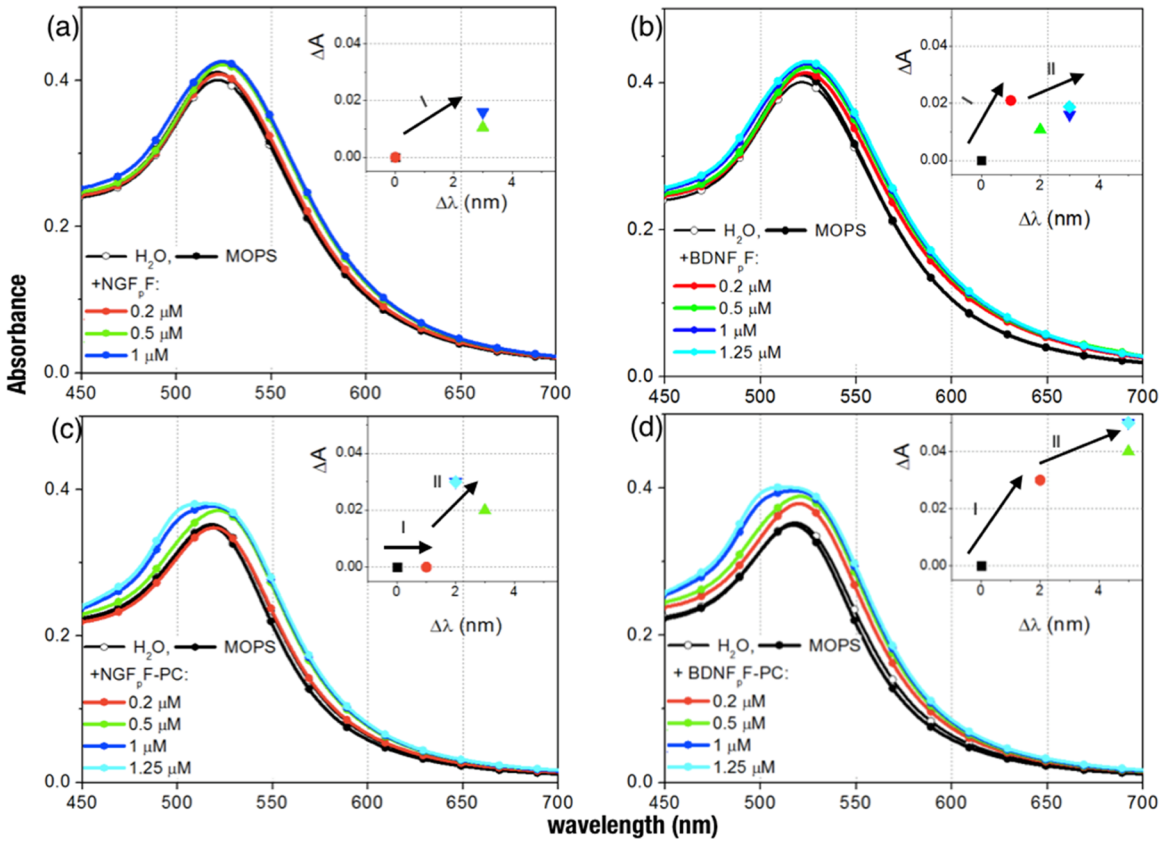

Figure 1. UV−vis spectra of AuNPs (2.2 nM) before (in water and in 3-(*N*-morpholino) propanesulfonic acid (MOPS) buffer) and after the addition of peptides at increasing concentrations (range, 2×10^{-7}−1.2×10^{-6} M) of (a) NGF_pF, (b) $BDNF_pF$, (c) NGF_pF-PC, and (d) $BDNF_pF$-PC. Insets: $\Delta A-\Delta\lambda$ scatter plots, with arrows indicating different steps of plasmon shifts (I, II). All experiments are conducted in triplicate.

and/or loosely bound peptide molecules from the peptide−AuNP hybrid systems (Figure S2) demonstrate a lower nanoparticle aggregation for the peptide-loaded SUVs/AuNPs in comparison with POPC SUVs (without peptide)/AuNPs.

In general, the centrifugation step, under the experimental conditions used, is efficient to collect, from the pellets, peptide-functionalized AuNPs (Figure S3). In particular, the comparison between the spectra of pellets and supernatants shows an almost totally irreversible adsorption for NGF_pF and $BDNF_pF$ in the direct interaction with the AuNPs. On the other hand, for the lipid-mediated interaction, as the spectra of supernatants clearly display spectral features of free peptides and/or peptide/PC systems, a partially reversible adsorption occurred. These findings indicate the possibility, through the lipid-mediated interaction, of modulating also the actual peptide coating onto AuNPs.

A semiquantitative estimation of the different interactions occurring between the two peptides and AuNPs can be obtained by the approximate nanoparticle coverage, calculated according to the peptide concentrations used to reach saturation in the UV−vis titration spectra. By considering spherical AuNPs with an average diameter (d) of 12 nm, the number of gold atoms can be calculated according to the formula: $N = d^3(\pi\rho/6M)$, where ρ is the density of fcc Au (19.3 g/cm^3) and M is the atomic weight (197 g/mol).[33] The corresponding coverages, in terms of peptide molecules for each AuNP, are about 1.2×10^7 and 2.4×10^7 for NGF_pF and $BDNF_pF$, respectively.

Because the molecular dimensions of NGF_pF and $BDNF_pF$ are $2.7 \times 1.7 \times 2.0$ nm^3 and $3.2 \times 1.7 \times 1.6$ nm^3, respectively, the ideal nanoparticle coverage by the peptides (in terms of peptide molecules/AuNP) ranges from ∼85 to ∼130 for NGF_pF and from ∼88 to ∼170 for $BDNF_pF$ in the two limit side-on and end-on configurations, respectively. Accordingly, "disordered" multilayers of NGF_pF molecules in side-on/end-on configuration (Scheme 1a) and more packed adlayers of $BDNF_pF$ molecules most likely in side-on configuration can be figured out at the interface with AuNP (Scheme 1b).

Although the stirring may also cause the coalescence of AuNPs and a population of aggregated nanoparticles cannot be excluded, the characterization of the pellets resuspended in the MOPS buffer evidences, however, significant peptide-dependent differences, as demonstrated by zeta-potential (ZP), dynamic light scattering (DLS), and atomic force microscopy (AFM) analyses.

In particular, Table 1 shows that all of the peptide-immobilized AuNPs display a comparable surface charge neutralization but actual changes in the hydrodynamic diameters.[34,35]

Indeed, negatively charged bare AuNPs exhibit a surface charge decrease of about 30−40% in the MOPS buffer with respect to the same particles dispersed in water, likely due to the partial charge neutralization of citrate anions surrounding the metal core[22] by the Na^+ and K^+ ions used to fix the ionic strength of the buffer. A major charge decrease (∼80%) of AuNPs is found after the interaction with the bare lipid vesicles, whereas the measured charge is null for all of the peptide/AuNP and peptide-PC/AuNP nanoparticles. This finding can be explained on the basis of the cationic character of both

DOI: 10.1021/acsomega.7b00458
ACS Omega 2017, 2, 4071−4079

Table 1. Hydrodynamic Size (Polydispersity Index (PI) within Brackets) and Surface Charge of Various AuNP Samples in MOPS Buffer

	average dimension (PI) (nm)	ZP (mV)
AuNP in water	25 ± 2 (0.5)	−60 ± 4
AuNP	32 ± 10 (0.6)	−37 ± 12
NGF_pF/AuNP	253 ± 34 (0.6)	∼0
$BDNF_pF$/AuNP	75 ± 3 (0.4)	∼0
PC	108 ± 5 (0.2)	∼0
NGF_pF-PC	122 ± 2 (0.2)	∼0
$BDNF_pF$-PC	104 ± 3 (0.3)	∼0
PC/AuNP	189 ± 29 (0.5)	−14 ± 5
NGF_pF-PC/AuNP	222 ± 122 (0.4)	∼0
$BDNF_pF$-PC/AuNP	80 ± 7 (0.3)	∼0

peptides (isoelectric pH of approximately 8−9[18]) under the experimental conditions used.

Interestingly, the hydrodynamic diameter of bare AuNPs (D = 26 ± 2 nm, in both water and the MOPS buffer) increases differently for NGF_pF/AuNP (250 ± 30 nm) and $BDNF_pF$/AuNP (75 ± 3 nm). According to the UV−vis data and the calculated nanoparticle coverage discussed above, these findings confirm the picture of peptide molecule multilayers organized, respectively, as extended (for NGF_pF) and compact (for $BDNF_pF$) adlayers at the interface with AuNPs.

Such a trend is also observed for lipid-loaded SUVs, where NGF_pF-PC exhibits a higher average diameter (D = 122 ± 2 nm) than $BDNF_pF$-PC (D = 104 ± 3 nm), which instead are comparable in size to control SUVs without peptide (D = 108 ± 5 nm). Therefore, NGF_pF molecules tend to an extended end-on-like arrangement, whereas $BDNF_pF$ molecules more likely lie flat on the leaflet plane of the lipid membrane.

As to the hybrid peptide−lipid/AuNP samples, hydrodynamic diameters of 172 ± 28 nm for NGF_pF-PC/AuNP (similar to 173 ± 34 nm measured for POPC SUV/AuNP) and 83 ± 7 nm for $BDNF_pF$-PC/AuNP are found. A possible explanation is that for the lipid-mediated interaction of NGF_pF with AuNP the lipids maintain their liposomal self-assembling state, whereas in the case of $BDNF_pF$, the interaction with the metal nanoparticle can prompt the formation of different lipid supramolecular assemblies (e.g., supported lipid bilayers, having a thickness of about 5 nm[36]).

The characterization of the peptide/AuNP samples in air by AFM analyses (Figure 2), although affected by additional aggregation effects because the samples were deposited on mica and dried, confirms, however, the actual nanoparticle coating by the peptides. In fact, from the height analysis of the particles, the average size of bare AuNPs (∼12 nm) increases up to ∼16 and ∼20 nm for NGF_pF/AuNP and $BDNF_pF$/AuNP, respectively. As to the peptide−lipid/AuNP samples, no relevant features could be detected on the solid-deposited samples, as the samples suffered the substrate effect on lipid assembly[36] (Figure S4).

The physicochemical characterization of the NGF_pF/AuNP and $BDNF_pF$/AuNP samples provided by X-ray photoelectron spectroscopy (XPS) further confirms the results obtained for the hybrid interfaces formed for the two peptides (Figure 3), with significant differences found for the peptide-immobilized samples with respect to bare AuNPs (Figure S5 and Table S1).

For the peak-fitting analysis of C 1s, the following four components are considered: C_1 (at a binding energy (BE) of 285.0 eV), due to C−C and C−H hydrocarbon bonds; C_2 (at a BE of 286.2 ± 0.2 eV), assigned to heterocarbon C−O and C−N bonds; and C_3 and C_4 (at BEs of 288.2 ± 0.2 and 289.0 ± 0.2 eV, due to C═O and C(═O)OH groups, respectively).[37]

Intrinsic structural differences due to the primary peptide sequence are clearly displayed in the carbon peak components found for NGF_pF (Figure 3b) and $BDNF_pF$ (Figure 3d). In fact, the ratio of polar to apolar components ($(C_2 + C_3 + C_4)/C_1$) exhibited by the former and the latter are 1.3 and 3.2,

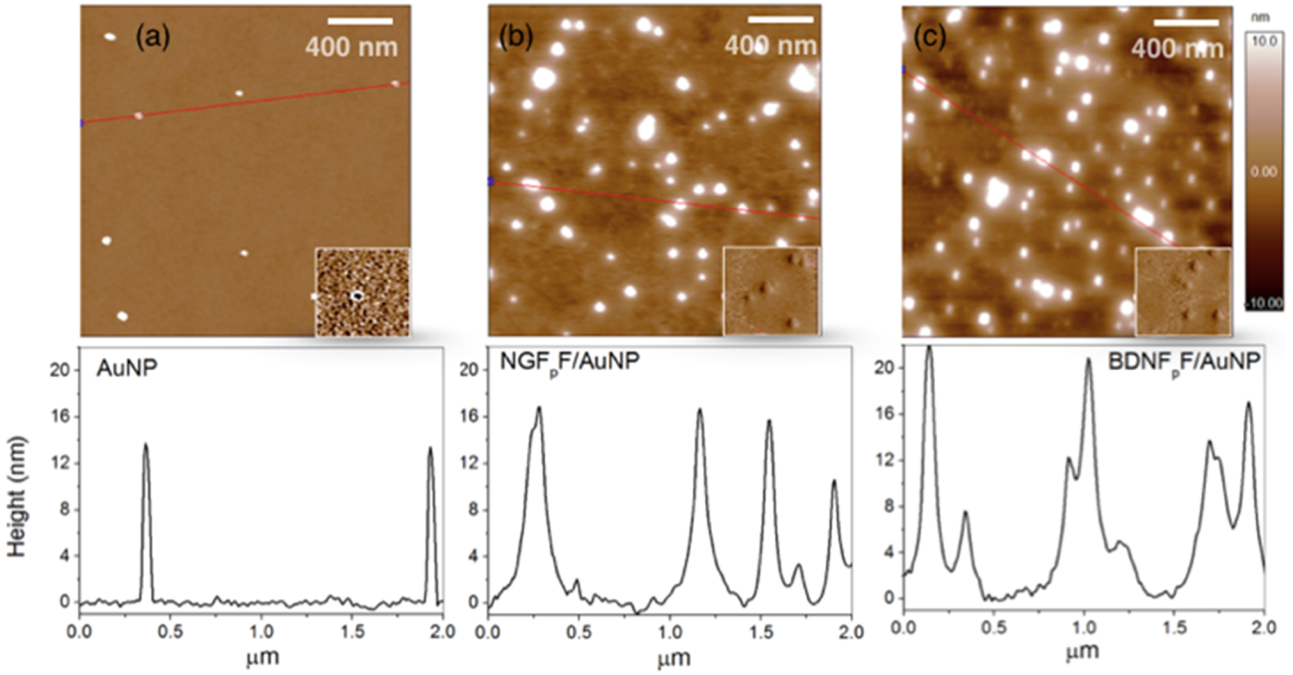

Figure 2. AFM topography images and height sections of (a) bare AuNP, (b) NGF_pF/AuNP, and (c) $BDNF_pF$/AuNP. Z scale = 20 nm. Insets show the corresponding phase images.

DOI: 10.1021/acsomega.7b00458
ACS Omega 2017, 2, 4071−4079

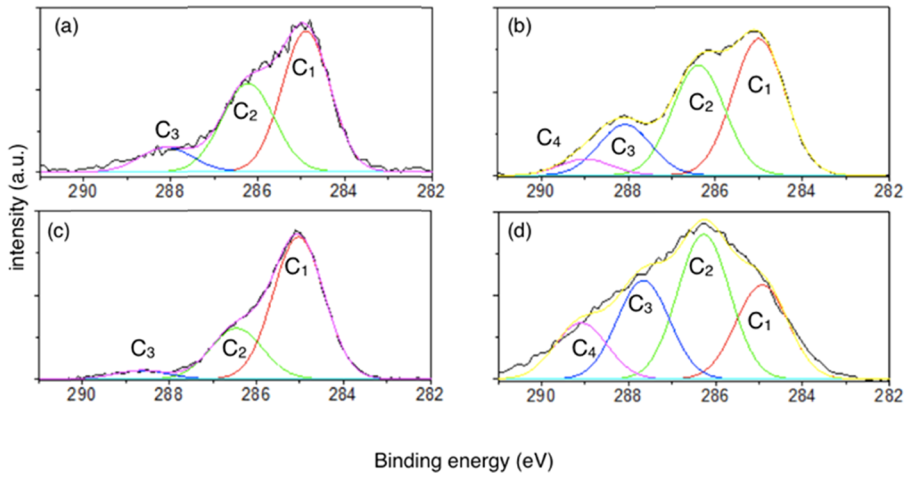

Figure 3. XPS peaks of C 1s for (a) NGF_pF/AuNP, (b) NGF_pF, (c) $BDNF_pF$/AuNP, and (d) $BDNF_pF$.

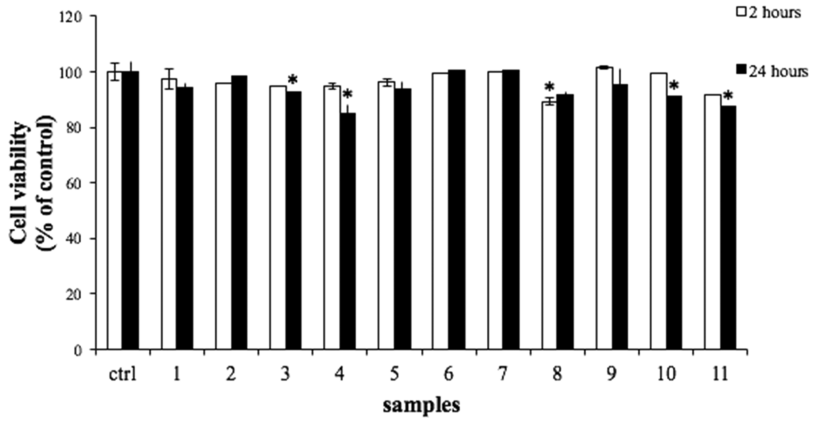

Figure 4. Viability assay on iHBMECs for samples (1) NGF_pF, (2) $BDNF_pF$, (3) POPC SUV, (4) NGF_pF-PC, (5) $BDNF_pF$-PC, (6) AuNP, (7) NGF_pF/AuNP, (8) NGF_pF-PC/AuNP, (9) $BDNF_pF$/AuNP, (10) $BDNF_pF$-PC/AuNP, and (11) POPC SUV/AuNPs. Statistical significance $*p < 0.05$ vs control.

respectively, according to the two extra amino acids in the NGF_pF sequence and also two more phenylalanine residues in comparison with $BDNF_pF$, which instead encompasses both one carboxylic residue and one guanidine extra residue.

Interestingly, the comparison of C 1s spectra for NGF_pF/AuNP (Figure 3a) and $BDNF_pF$/AuNP (Figure 3c) samples suggest that the BDNF peptide molecules bind to the gold surface predominantly through the guanidine, carbonyl, and carboxyl groups (i.e., strong decrease of C_2, C_3, and C_4 components, respectively), according to the picture of molecules lying at the interface in the extended side-on arrangement. In the case of the NGF peptide, a minor change in the peak shape can be an indicator of a more localized interaction among certain sites of the peptide sequence and the AuNP, which results in a less ordered hybrid interface.

To test the transport of neurotrophin-peptide-functionalized AuNPs across the BBB, a cellular model of immortalized human brain microvascular endothelial cells (iHBMECs) was used. The HBMEC model is representative of human brain endothelium and exhibits barrier properties comparable to other BBB models.[38] First, cell viability was assessed to verify that the various peptide/lipid/AuNP assemblies were nontoxic under the experimental conditions used. No toxicity was found up to 24 h of cell treatment (Figure 4).

Second, as it is well known that AuNPs are capable of crossing the BBB,[15] the effect of the nanoparticle functionalization was here scrutinized in terms of cell internalization by the various peptide/lipid/AuNP assemblies, to find differences (if any) depending on the peptides and/or the immobilization approaches, for example, direct or lipid-mediated adsorption, used for tailoring the AuNPs.

Figure 5 shows the representative images of laser scanning confocal microscopy (LSM) for cells incubated for 2 h with NGF_pF and $BDNF_pF$ (emitting in the green, due to Fam moieties): free (Figure 5a), immobilized on AuNPs by direct adsorption (Figure 5b), loaded in rhodamine-labeled POPC SUVs (emitting in the red; Figure 5c), and immobilized on AuNPs by lipid-mediated adsorption (Figure 5d).

An enhancement of peptide internalization by the cells in the functionalized AuNPs compared with both free peptides and peptide-loaded SUVs is visible. Interestingly, for NGF_pF/AuNP, a higher peptide uptake (displayed by a diffuse green emission in the cytoplasm) and intracellular aggregation of the AuNPs (dark spots in the optical micrograph; open arrows in Figure 5b) is found compared to that for $BDNF_pF$/AuNP. This latter exhibits a more localized distribution (dotted green emission), with a preferential localization at the cell membrane (solid arrow in Figure 5b). As to NGF_pF-PC/AuNP and $BDNF_pF$-PC/AuNP systems, the cellular internalization is

DOI: 10.1021/acsomega.7b00458
ACS Omega 2017, 2, 4071−4079

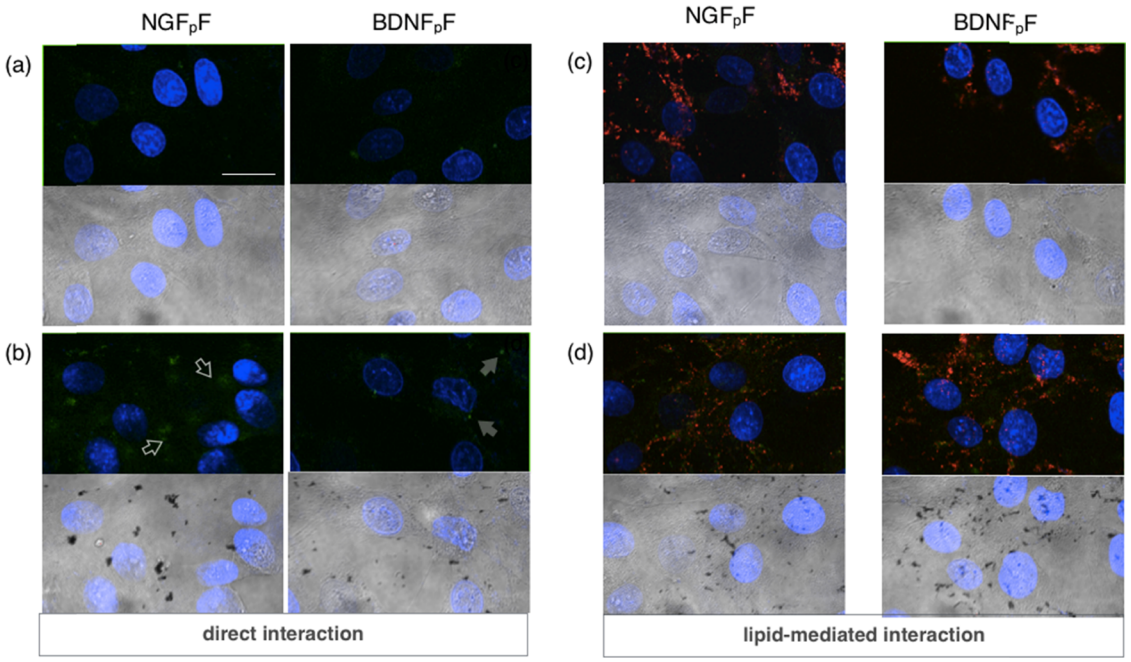

Figure 5. LSM images of iHBMECs incubated for 2 h (37 °C, 5% CO_2) with (a) NGF$_p$F (or BDNF$_p$F), (b) NGF$_p$F (or BDNF$_p$F)/AuNP, (c) NGF$_p$F-PC (or BDNF$_p$F-PC), and (d) NGF$_p$F-PC (or BDNF$_p$F-PC)/AuNP. Scale bar = 20 μm. Each sample consists of merged fluorescence images of nuclei (blue; DAPI, $\lambda_{ex/em}$ = 405/425−475 nm), peptides (green; Fam, $\lambda_{ex/em}$ = 488/500−530 nm), and lipids (red; rhodamine, $\lambda_{ex/em}$ = 543/550−650 nm) (top panels) and merged DAPI emission and optical bright-field images (bottom panels).

comparable for both peptides, with green spots co-localizing with the AuNPs, also in the nuclei.

3. CONCLUSIONS

In summary, we set up a new promising approach to develop a "tunable" multifunctional platform based on a neurotrophin-like potential drug (NGF and BDNF peptides) and a plasmonic/fluorescence image-contrast working principle. A modulation in the peptide immobilization was demonstrated by a comparative study (by UV−vis, AFM, DLS, and ZP analyses) of direct and lipid-mediated peptide−AuNP interaction. Further physicochemical and biological (including in vivo test) studies on these hybrid nanobiointerfaces will be necessary to accurately control the subcellular localization of the drug and to quantify the actual capability of crossing the BBB.

4. EXPERIMENTAL METHODS

4.1. Materials. Ultrapure Milli-Q water (resistivity > 18 MΩ cm^{-1}) was used for all experiments. Glassware was cleaned immediately before use by immersing in aqua regia (HCl:HNO_3, 3:1 volume ratio), followed by rinsing with copious amount of water. Hydrogen tetrachloroaurate ($HAuCl_4$) and trisodium citrate dihydrate ($Na_3C_6H_5O_7 \cdot 2H_2O$, TSC) were purchased from Sigma-Aldrich.

4.1.1. Buffers. The phosphate-buffered saline (PBS) solution (pH = 7.4 at 25 °C) was prepared by dissolving PBS tablets (0.01 M phosphate, 2.7 mM KCl, 137 mM NaCl, purchased from Sigma-Aldrich) in ultrapure water. The MOPS buffer solution (added with 0.27 mM KCl and 13.7 mM NaCl) was prepared at a concentration of 1 mM, with pH corrected to 7.4 (25 °C).

4.1.2. Peptides. The N-terminal fragments (1−14) of NGF (NGF1-14) and (1−12) of BDNF (BDNF1-12) peptides[39,40] were purchased from Caslo (Lyngby, Denmark) as lyophilized powders (purity > 95%).

To dye-label the peptide with the fluorescein (Fam) group ($\lambda_{ex}/\lambda_{em}$ = 488/520 nm), a lysine (Lys) was added at the C-terminus of the peptides sequences, to obtain SSSHPIFHR-GEFSV-K-Fam (named NGF$_p$F) and HSDPARRGELSV-K-Fam (named BDNF$_p$F). Stock peptide samples were prepared at a concentration of 10^{-3} M in Milli-Q water and stored at −20 °C.

4.1.3. Lipids. 1-Palmitoyl-2-oleoyl-*sn*-glycero-3-phosphocholine (POPC) and rhodamine-labeled 1,2-dihexadecanoyl-*sn*-glycero-3-(Rhod-DHPE) phospholipids in chloroform were purchased from Avanti Polar Lipids (Alabaster, AL).

4.2. Preparation of SUV and Peptide/SUV Systems. A chloroform solution of POPC (5 mg/mL) and Rhod-DHPE (1 wt %) was taken in a round-bottom flask, and, after evaporating the solvent under argon flow, the dried lipid film formed on the wall of the flask was emulsified in PBS (to obtain SUV) or 0.5 mM peptide solution in PBS (to obtain N-Fam/SUV or B-Fam/SUV) and vortexed. The lipid dispersions were therefore extruded 13 times through a 100 nm polycarbonate membrane, followed by another 13 times through a 30 nm membrane (Avanti Polar Lipids).

To remove unloaded peptide molecules from the peptide/SUV systems, Amicon Ultra-0.5 ultracentrifuge filters (Sigma-Aldrich)[41] were used to centrifuge (14 000 rpm for 30 min at 25 °C) and the recovered solutions were characterized (Figure S1). The SUV and peptide/SUVs were stored under Ar and used within 2 weeks, according to an established protocol.[42]

4.3. Preparation of Hybrid Peptide(/SUV)/AuNP. AuNPs were synthesized by chemical reduction of HAuCl4 (1 mM) with TSC (1 wt %). The plasmonic band centered at 518 nm and the full width at half-maximum of about 50 nm confirmed the formation of monodisperse spherical gold colloids with a diameter of 12 nm.[43,44] N-Fam(/SUV)/AuNP

DOI: 10.1021/acsomega.7b00458
ACS Omega 2017, 2, 4071−4079

and B-Fam(/SUV)/AuNP were prepared by adding 10^{-6} M peptide (or peptide-loaded SUV) solutions to AuNP at a concentration of 2.2 nM in 1 mM MOPS. After vigorous stirring and about 5 min of incubation, the mixtures were centrifuged (8000 rpm for 15 min at 25 °C); the recovered pellets were redissolved in 1 mM MOPS and used for the characterization as well as cell treatments.

4.4. Physicochemical Characterization. *4.4.1. UV−Vis.* A Jasco V-650 spectrophotometer was used, with quartz cuvettes having an optical path length of 1 cm.

4.4.2. DLS and ZP. A NanoPartica SZ-100 apparatus equipped with a 514 nm "green" laser from HORIBA Scientific was used. Reproducibility was verified by collection and comparison of sequential measurements in at least three separate series of experiments. The samples were not filtered before measurements. At least five measurements were made for each sample and data averaged.

4.4.3. AFM. For AFM analyses, drops (20 μL) of the various peptide/AuNP samples were allowed to adsorb at room temperature on freshly cleaved muscovite mica (Ted Pella, Inc.). After 5 min, the mica surface was briefly washed with 100 μL of ultrapure water, dried under a gentle nitrogen stream, and immediately imaged. A Cypher AFM instrument (Asylum Research, Oxford Instruments, Santa Barbara, CA) operating in tapping or AC mode and equipped with a scanner at an XY scan range of 30/40 μm (closed/open loop) was used. Silicon tetrahedral tips mounted on 30 μm long rectangular cantilevers were purchased from Olympus (AT240TS; Oxford Instruments). The probes had a nominal spring constant of 2 N/m and a driving frequency of 70 kHz. A number of images covering 1−5 μm^2 surfaces were scanned, and the lengths of particles were measured using a freehand tool in the MFP-3DTM offline section analysis software. The same tool was used to measure the cross sections of particles.

4.4.4. XPS. XPS measurements were performed using a PHI 5000 VersaProbe apparatus equipped with a monochromatic Al Kα source (1486.7 eV). Typically, the pressure in the analysis chamber was 5×10^{-9} torr. The dual-beam charge neutralization method with electron (∼1 eV) and argon ion (<10 eV) guns was used for charge compensation. Au 4f, C 1s, O 1s, N 1s, and S 2p signals were acquired at a constant pass energy and an analyzer energy step of 23.5 and 0.2 eV, respectively. Fitting was then realized with software provided by PHI, with preliminary Shirley background subtraction. Each spectrum is referenced to a carbon pollution at 285.0 eV of BE. All BE values are given at ±0.2 eV.

4.5. Cellular Experiments. *4.5.1. Cell Cultures.* Monolayers of iHBMEC (Innoprot, Elexalde Derio, Spain) were fed with endothelial basal medium, supplemented with 5% fetal bovine serum, 1% endothelial cell growth supplement, 100 U/mL penicillin, and 100 mg/mL streptomycin.

4.5.2. Cell Viability Assays. To evaluate cell viability in ECs, the 3-[4,5-dimethylthiazol-2-yl]-2,5-diphenyl tetrasodium bromide (MTT) assay was used (Chemicon, Temecula, CA). The cells (10 000 cells/well) were plated in 96-well plates and grown in complete medium, in the absence (control cells) or presence of bare or peptide-functionalized AuNPs at a final concentration of 3 nM for 2 and 24 h. At the end of treatment, the cells were incubated with MTT for 3 h, 100 μL of dimethyl sulfoxide was added, and the absorbance was measured at 590 nm, as previously described.[45]

4.5.3. Model Experiment of BBB Crossing by LSM Analyses. At confluence, cells were split on glass-bottom Petri dishes (WillCo Wells; glass diameter, 22 mm) pretreated with a mixture of 30 ng/mL collagen and 10 ng/mL fibronectin (1 h, room temperature), to allow cell adhesion (2×10^4 cells/well). The day after, the cells were treated with the various samples at a final concentration of 3.0×10^{-9} M of the AuNPs. After 2 h of incubation, the cells were washed with the PBS solution (10 mM PBS, 37 °C, pH = 7.4), fixed, and stained with the nuclear dye DAPI (ThermoFisher).

LSM was performed with an Olympus FV1000 confocal laser scanning microscope, equipped with diode UV (405 nm, 50 mW), multiline argon (457, 488, and 515 nm; total, 30 mW), HeNe(G) (543 nm, 1 mW), and HeNe(R) (633 nm, 1 mW) lasers. An oil-immersion objective (60xO PLAPON) and spectral filtering system was used. The detector gain was fixed at a constant value, and images were taken, in a sequential mode, for all of the samples at random locations throughout the area of the well.

■ ASSOCIATED CONTENT

Supporting Information

The Supporting Information is available free of charge on the ACS Publications website at DOI: 10.1021/acsomega.7b00458.

Analyses of centrifugates and UV−vis spectra (Figures S1−S3); AFM analysis of peptide(lipid)/AuNP sample (Figure S4); quantitative XPS analysis (Table S1); deconvolution analysis of XPS C 1s peak for bare AuNPs (Figure S5) (PDF)

■ AUTHOR INFORMATION

Corresponding Authors

*E-mail: lamendola@farm.unipi.it. Tel: +39 050 2219533. Fax: +39 050 2210680 (D.L.M.).

*E-mail: csatriano@unict.it. Tel: +39 095 7385136. Fax: +39 095 580138 (C.S.).

ORCID

Cristina Satriano: 0000-0001-5348-5863

Author Contributions

The manuscript was written through contributions of all authors. All authors have given approval to the final version of the manuscript.

Notes

The authors declare no competing financial interest.

■ ACKNOWLEDGMENTS

The authors acknowledge MIUR funding (PRIN2015_20152EKS4Y) and Consorzio Interuniversitario di Ricerca sulla Chimica dei Metalli nei Sistemi Biologici (CIRCMSB).

■ REFERENCES

(1) Saraiva, C.; Praça, C.; Ferreira, R.; Santos, T.; Ferreira, L.; Bernardino, L. Nanoparticle-mediated brain drug delivery: Overcoming blood−brain barrier to treat neurodegenerative diseases. *J. Controlled Release* **2016**, *235*, 34−47.

(2) Cupaioli, F. A.; Zucca, F. A.; Boraschi, D.; Zecca, L. Engineered nanoparticles. How brain friendly is this new guest? *Prog. Neurobiol.* **2014**, *119-120*, 20−38.

(3) Huang, E. J.; Reichardt, L. F. Neurotrophins: roles in neuronal development and function. *Annu. Rev. Neurosci.* **2001**, *24*, 677−736.

(4) Bothwell, M. NGF, BDNF, NT3, and NT4. *Handb. Exp. Pharmacol.* **2014**, *220*, 3−15.

DOI: 10.1021/acsomega.7b00458
ACS Omega 2017, 2, 4071−4079

(5) Steiner, J. P.; Nath, A. Neurotrophin strategies for neuroprotection: are they sufficient? *J. Neuroimmune Pharmacol.* **2014**, *9*, 182−94.
(6) Josephy-Hernandez, S.; Jmaeff, S.; Pirvulescu, I.; Aboulkassim, T.; Saragovi, H. U. Neurotrophin receptor agonists and antagonists as therapeutic agents: An evolving paradigm. *Neurobiol. Dis.* **2017**, *97*, 139−155.
(7) Vilar, M.; Mira, H. Regulation of Neurogenesis by Neurotrophins during Adulthood: Expected and Unexpected Roles. *Front. Neurosci.* **2016**, *10*, 26.
(8) Weissmiller, A. M.; Wu, C. Current advances in using neurotrophic factors to treat neurodegenerative disorders. *Transl. Neurodegener.* **2012**, *1*, 14.
(9) Makani, V.; Jang, Y. G.; Christopher, K.; Judy, W.; Eckstein, J.; Hensley, K.; Chiaia, N.; Kim, D. S.; Park, J. BBB-Permeable, Neuroprotective, and Neurotrophic Polysaccharide, Midi-GAGR. *PLoS One* **2016**, *11*, No. e0149715.
(10) Pardridge, W. M. The blood-brain barrier: bottleneck in brain drug development. *NeuroRx* **2005**, *2*, 3−14.
(11) Pandini, G.; Satriano, C.; Pietropaolo, A.; Giani, F.; Travaglia, A.; La Mendola, D.; Nicoletti, V. G.; Rizzarelli, E. The Inorganic Side of NGF: Copper(II) and Zinc(II) Affect the NGF Mimicking Signaling of the N-Terminus Peptides Encompassing the Recognition Domain of TrkA Receptor. *Front. Neurosci.* **2016**, *10*, 569.
(12) Velasco-Aguirre, C.; Morales, F.; Gallardo-Toledo, E.; Guerrero, S.; Giralt, E.; Araya, E.; Kogan, M. J. Peptides and proteins used to enhance gold nanoparticle delivery to the brain: preclinical approaches. *Int. J. Nanomed.* **2015**, *10*, 4919−36.
(13) Maus, L.; Dick, O.; Bading, H.; Spatz, J. P.; Fiammengo, R. Conjugation of Peptides to the Passivation Shell of Gold Nanoparticles for Targeting of Cell-Surface Receptors. *ACS Nano* **2010**, *4*, 6617−6628.
(14) Goldsmith, M.; Abramovitz, L.; Peer, D. Precision Nanomedicine in Neurodegenerative Diseases. *ACS Nano* **2014**, *8*, 1958−1965.
(15) Sela, H.; Cohen, H.; Elia, P.; Zach, R.; Karpas, Z.; Zeiri, Y. Spontaneous penetration of gold nanoparticles through the blood brain barrier (BBB). *J. Nanobiotechnol.* **2015**, *13*, 71.
(16) Sánchez-López, E.; Ettcheto, M.; Egea, M. A.; Espina, M.; Calpena, A. C.; Folch, J.; Camins, A.; Garcia, M. L. New potential strategies for Alzheimer's disease prevention: pegylated biodegradable dexibuprofen nanospheres administration to APPswe/PS1dE9. *Nanomedicine* **2017**, *13*, 1171−1182.
(17) Wilson, C. M.; Magnaudeix, A.; Naves, T.; Vincent, F.; Lalloue, F.; Jauberteau, M. O. The Ins and Outs of Nanoparticle Technology in Neurodegenerative Diseases and Cancer. *Curr. Drug Metab.* **2015**, *16*, 609−632.
(18) Forte, G.; Travaglia, A.; Magri, A.; Satriano, C.; La Mendola, D. Adsorption of NGF and BDNF derived peptides on gold surfaces. *Phys. Chem. Chem. Phys.* **2014**, *16*, 1536−1544.
(19) Satriano, C.; Forte, G.; Magri, A.; Di Pietro, P.; Travaglia, A.; Pandini, G.; Giani, F.; La Mendola, D. Neurotrophin-mimicking peptides at the biointerface with gold respond to copper ion stimuli. *Phys. Chem. Chem. Phys.* **2016**, *18*, 30595−30604.
(20) Gupta, A.; Moyano, D. F.; Parnsubsakul, A.; Papadopoulos, A.; Wang, L. S.; Landis, R. F.; Das, R.; Rotello, V. M. Ultrastable and Biofunctionalizable Gold Nanoparticles. *ACS Appl. Mater. Interfaces* **2016**, *8*, 14096−101.
(21) Pan, Y.; Ding, H.; Qin, L.; Zhao, X.; Cai, J.; Du, B. Gold nanoparticles induce nanostructural reorganization of VEGFR2 to repress angiogenesis. *J. Biomed. Nanotechnol.* **2013**, *9*, 1746−56.
(22) Di Pietro, P.; Strano, G.; Zuccarello, L.; Satriano, C. Gold and Silver Nanoparticles for Applications in Theranostics. *Curr. Top. Med. Chem.* **2016**, *16*, 3069−3102.
(23) Alfranca, G.; Artiga, A.; Stepien, G.; Moros, M.; Mitchell, S. G.; de la Fuente, J. M. Gold nanoprism-nanorod face off: comparing the heating efficiency, cellular internalization and thermoablation capacity. *Nanomedicine* **2016**, *11*, 2903−2916.
(24) Cho, S.; Shin, H. Y.; Kim, M. I. Nanohybrids consisting of magnetic nanoparticles and gold nanoclusters as effective peroxidase mimics and their application for colorimetric detection of glucose. *Biointerphases* **2017**, *12*, No. 01A401.
(25) Kairdolf, B. A.; Qian, X.; Nie, S. Bioconjugated Nanoparticles for Biosensing, In-Vivo Imaging, and Medical Diagnostics. *Anal. Chem.* **2016**, *89*, 1015−1031.
(26) Daneman, R. The blood-brain barrier in health and disease. *Ann. Neurol.* **2012**, *72*, 648−72.
(27) Liu, S.; Agalliu, D.; Yu, C.; Fisher, M. The role of pericytes in blood-brain barrier function and stroke. *Curr. Pharm. Des.* **2012**, *18*, 3653−62.
(28) Di Pietro, P.; Zaccaro, L.; Comegna, D.; Del Gatto, A.; Saviano, M.; Snyders, R.; Cossement, D.; Satriano, C.; Rizzarelli, E. Silver nanoparticles functionalized with a fluorescent cyclic RGD peptide: a versatile integrin targeting platform for cells and bacteria. *RSC Adv.* **2016**, *6*, 112381−112392.
(29) Kim, H. M.; Jin, S. M.; Lee, S. K.; Kim, M. G.; Shin, Y. B. Detection of Biomolecular Binding Through Enhancement of Localized Surface Plasmon Resonance (LSPR) by Gold Nanoparticles. *Sensors* **2009**, *9*, 2334−44.
(30) Kelly, K. L.; Coronado, E.; Zhao, L. L.; Schatz, G. C. The Optical Properties of Metal Nanoparticles: The Influence of Size, Shape, and Dielectric Environment. *J. Phys. Chem. B* **2003**, *107*, 668−677.
(31) Zhao, P.; Li, N.; Astruc, D. State of the art in gold nanoparticle synthesis. *Coord. Chem. Rev.* **2013**, *257*, 638−665.
(32) Zuccarello, L.; Rampazzo, E.; Petrizza, L.; Prodi, L.; Satriano, C. The influence of fluorescent silica nanoparticle surface chemistry on the energy transfer processes with lipid bilayers. *RSC Adv.* **2016**, *6*, 52674−52682.
(33) Liu, X.; Atwater, M.; Wang, J.; Huo, Q. Extinction coefficient of gold nanoparticles with different sizes and different capping ligands. *Colloids Surf., B* **2007**, *58*, 3−7.
(34) Esfahani, M. R.; Pallem, V. L.; Stretz, H. A.; Wells, M. J. Extinction, emission, and scattering spectroscopy of 5−50 nm citrate-coated gold nanoparticles: An argument for curvature effects on aggregation. *Spectrochim. Acta, Part A* **2017**, *175*, 100−109.
(35) Piella, J.; Bastus, N. G.; Puntes, V. Size-Dependent Protein-Nanoparticle Interactions in Citrate-Stabilized Gold Nanoparticles: The Emergence of the Protein Corona. *Bioconjugate Chem.* **2017**, *28*, 88−97.
(36) Satriano, C.; Edvardsson, M.; Ohlsson, G.; Wang, G.; Svedhem, S.; Kasemo, B. Plasma oxidized polyhydroxymethylsiloxane–a new smooth surface for supported lipid bilayer formation. *Langmuir* **2010**, *26*, 5715−25.
(37) Bhagwat, N.; Murray, R. E.; Shah, S. I.; Kiick, K. L.; Martin, D. C. Biofunctionalization of PEDOT films with laminin-derived peptides. *Acta Biomater.* **2016**, *41*, 235−46.
(38) Bachmeier, C.; Mullan, M.; Paris, D. Characterization and use of human brain microvascular endothelial cells to examine beta-amyloid exchange in the blood-brain barrier. *Cytotechnology* **2010**, *62*, 519−29.
(39) Travaglia, A.; Satriano, C.; Giuffrida, M. L.; La Mendola, D.; Rampazzo, E.; Prodi, L.; Rizzarelli, E. Electrostatically driven interaction of silica-supported lipid bilayer nanoplatforms and a nerve growth factor-mimicking peptide. *Soft Matter* **2013**, *9*, 4648.
(40) Travaglia, A.; La Mendola, D.; Magrì, A.; Nicoletti, V. G.; Pietropaolo, A.; Rizzarelli, E. Copper, BDNF and Its N-terminal Domain: Inorganic Features and Biological Perspectives. *Chem. − Eur. J.* **2012**, *18*, 15618−15631.
(41) Catania, A.; Barrajon-Catalan, E.; Nicolosi, S.; Cicirata, F.; Micol, V. Immunoliposome encapsulation increases cytotoxic activity and selectivity of curcumin and resveratrol against HER2 over-expressing human breast cancer cells. *Breast Cancer Res. Treat.* **2013**, *141*, 55−65.
(42) Satriano, C.; Svedhem, S.; Kasemo, B. Well-defined lipid interfaces for protein adsorption studies. *Phys. Chem. Chem. Phys.* **2012**, *14*, 16695−8.

DOI: 10.1021/acsomega.7b00458
ACS Omega 2017, 2, 4071−4079

(43) Turkevich, J.; Stevenson, P. C.; Hillier, J. A study of the nucleation and growth processes in the synthesis of colloidal gold. *Discuss. Faraday Soc.* **1951**, *11*, 55.
(44) Frens, G. Controlled Nucleation for the Regulation of the Particle Size in Monodisperse Gold Suspensions. *Nat. Phys. Sci.* **1973**, *241*, 20−22.
(45) Tibullo, D.; Caporarello, N.; Giallongo, C.; Anfuso, C.; Genovese, C.; Arlotta, C.; Puglisi, F.; Parrinello, N.; Bramanti, V.; Romano, A.; Lupo, G.; Toscano, V.; Avola, R.; Brundo, M.; Di Raimondo, F.; Raccuia, S. Antiproliferative and Antiangiogenic Effects of Punica granatum Juice (PGJ) in Multiple Myeloma (MM). *Nutrients* **2016**, *8*, 611.

DOI: 10.1021/acsomega.7b00458
ACS Omega 2017, 2, 4071−4079